Workshop ***Waves in Porous Media***
IGPUBA, Facultad de Ingeniería, UBA, 5-10-2023

Calibration of a poroelastic rock physics model from well logs and cuttings: a case study from Inoceramus shale, Austral basin, Argentina

Claudia L. Ravazzoli,
Facultad de Ciencias Astronómicas y Geofísicas, UNLP y CONICET
Guido Panizza,
YPF-Tecnología S.A. y CONICET

Acknowledgements

The contents of this talk were part of Dr. Guido Panizza Phd Thesis, recently approved at the Faculty of Astronomical and Geophysical Sciences of National University of La Plata, Argentina, developed at YPF Tecnología S.A. with a co-funded scholarship CONICET – Y-TEC.

http://sedici.unlp.edu.ar/handle/10915/154026

Introduction

- Shales compose a large part of sedimentary basins worldwide.
- They are cap rocks in hydrocarbon reservoirs, seals for carbon sequestration and repositories for nuclear waste.
- Organic-rich shales are also important as petroleum source rocks and as unconventional resources.
- In Argentina, shale reservoirs represent 40% of the country's oil reserves and about 60% of its gas reserves.
- Recent experimental works demonstrate the high potential of organic rich shales for carbon dioxide sequestration, through adsorption processes.

Motivations

- The evaluation of elastic and geomechanic coefficients in these rocks at well scale is needed for their characterization and also for planning drilling and production strategies.

- This is very important in unconventional organic rich shale reservoirs such as Inoceramus formation, the main source rock in Austral Basin, Argentina.

- In previous studies we described and quantified the *elastic anisotropy of Inoceramus* shales (Panizza et al. 2022), using core plugs and ultrasonic velocities.

- Well logs do not provide enough information to determine the whole stiffness (or compliance) tensors. **We show that rock physics tools are highly useful for this problems.**

Main goals

- We propose a **workflow** for the calibration of a poroelastic velocity model at *in situ differential stress conditions*, using well logs and laboratory measurements on cuttings.

- Our model is based on a combination of the theory *porosity-deformation approach* (Shapiro & Kaselow 2005, Shapiro, 2017) and Ciz & Shapiro (2007).

- The calibration procedure involves the utilization of an inversion method to determine model fitting coefficients and physical properties of the organic matter (kerogen).

Elastic anisotropy in organic shales

Seismic anisotropy in shales may be due to different causes:

- preferred orientation (*texture*) of clay particles
- fine layering
- cracks and microcracks
- stress-induced anisotropy
- alignment of low aspect ratio pores
- other

The relationship between petrophysical properties of shales and their elastic behavior is complex.

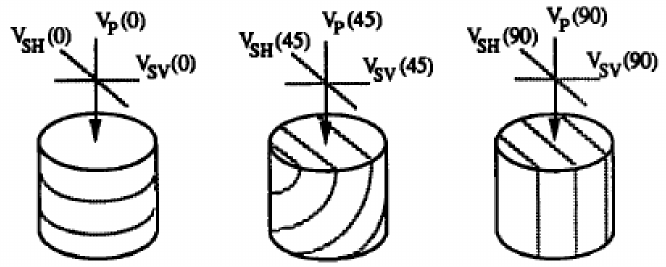

FIG. 1. Scheme of sample preparation and velocity measurements in shales. Wave propagation and polarization with respect to bedding-parallel lamination is shown. Numbers in parentheses indicate the phase velocity angle θ with respect to the bedding-normal symmetry axis.

Vernik & Nur 1992

Organic Matter in Shales

- This is measured by means of **Total Organic Content TOC** coefficient (in lab or wells).
- *Kerogen* is an amorphous porous solid of different types.
- Its porosity increases with maturation.
- The amount of kerogen in the rock affects its density, elastic and electric properties and consequently, is important in rock physics.
- So, we need to compute the volume fraction occupied by kerogen in the form:

$$K = \frac{TOC}{C_K} \frac{\rho_{gr}}{\rho_K}$$

$$\rho_{gr}, \rho_K : grain, kerogen\ densities$$

$$C_K = \frac{mass\ organic\ Carbon}{kerogen\ mass}$$

Kerogen may have uncertain physical and geochemical parameters

VTI anisotropy – notation

Generalized Hooke' s Law $\sigma_{ij} = c_{ijkl}\varepsilon_{kl}$ $\varepsilon_{ij} = S_{ijkl}\sigma_{kl}$

c_{ijkl} Stiffness tensor

S_{ijkl} Compliance tensor

$$S = (C)^{-1}$$

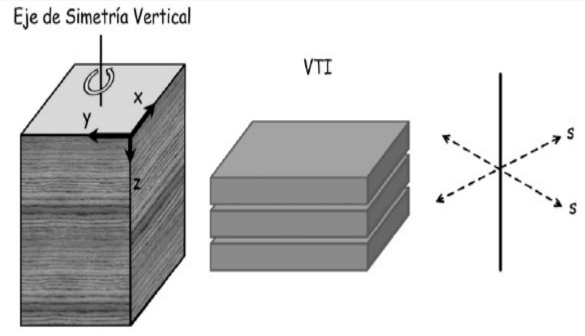

VTI Symmetry – Voigt notation

$$C_{IJ} = \begin{pmatrix} C_{11} & C_{12} & C_{13} & 0 & 0 & 0 \\ & C_{11} & C_{13} & 0 & 0 & 0 \\ & & C_{33} & 0 & 0 & 0 \\ & & & C_{44} & 0 & 0 \\ & & & & C_{44} & 0 \\ & & & & & C_{66} \end{pmatrix}$$

$$C_{12} = C_{11} - 2C_{66}$$

Strain Energy restrictions

(1) $C_{11} > |C_{12}|$ (2) $(C_{11} + C_{12})C_{33} > 2C_{13}^2$ (3) $C_{44} > 0$

Long-wavelength hypothesis

- The wavelengths of sonic waves are on the order of tens of centimeters.
- The grain sizes are in the order of 10^{-2} to 10^{-1} mm.
- Pores and cracks are in the sub-microscopic scale (micrometric, nanometric pores).
- Thus, they are much bigger than the characteristic dimensions of the heterogeneities of the rock.
- So, we will assume that a *long-wavelength* assumption is reasonable for this study, valid for a fixed sonic frequency.

Stress dependent anisotropic elastic model for the dry rock matrix: **Porosity Deformation Approach**

Shapiro (2003), Shapiro & Kaselow, (2005), Shapiro (2017)

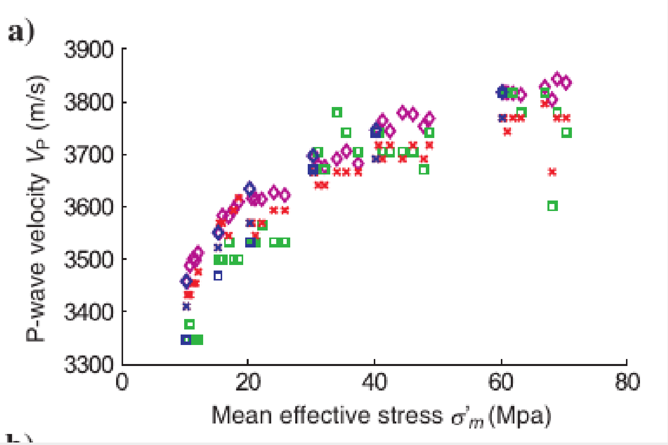

Porosity-Deformation Approach

For a proper calibration of the model we need to take into account the *in situ* conditions of the rocks → stress and pore pressure dependent model.

The Differential Stress dependence of seismic wave velocities is phenomenologically approximated in the form (for dry and saturated rocks):

$$V(P_d) = A + B P_d - C e^{-P_d D}$$

non linear relation, progressive closure of compliant porosity with increasing differential stress

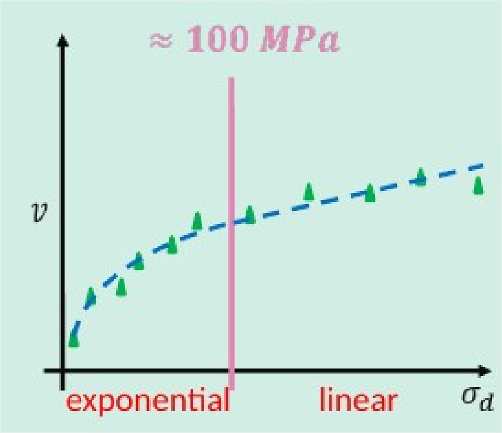

Based on a **Dual Porosity concept**, Shapiro split the pore volume as :

$$\phi = \phi_s + \phi_c$$

Stiff pores and Compliant pores

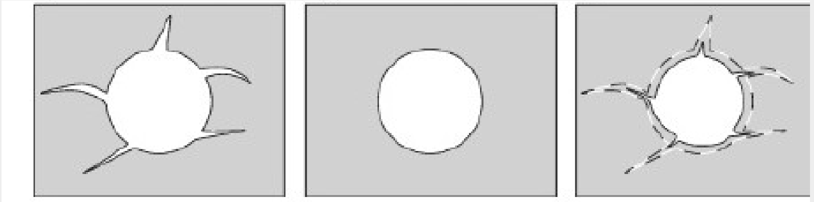

Piezosensitivity PDA model

Using the "*piezosensitivity*" approach, he found that this nonlinear behavior of rocks can be well explained by the strain of compliant pores.

After lengthy calculations, in simplified form, for **VTI** symmetry the compliance tensor of the matrix can be written as

$$
\begin{aligned}
S_{11}^{m} &= a_{11} + b_{11} F_c\, e^{-F_c \sigma_1^d}, \\
S_{33}^{m} &= a_{33} + b_{33} F_c\, e^{-F_c \sigma_3^d}, \\
S_{44}^{m} &= a_{44} + \frac{F_c}{4}\left(b_{22}\, e^{-F_c \sigma_2^d} + b_{33}\, e^{-F_c \sigma_3^d}\right), \\
S_{66}^{m} &= a_{66} + \frac{F_c}{4}\left(b_{11}\, e^{-F_c \sigma_1^d} + b_{22}\, e^{-F_c \sigma_2^d}\right), \\
S_{13}^{m} &= a_{13}
\end{aligned}
$$

where $\sigma_1^d, \sigma_2^d, \sigma_3^d$ are the differential stress in the principal directions.

Involving 9 fitting parameters

$$\mathbf{m} = (a_{11}, a_{13}, a_{33}, a_{44}, a_{66}, b_{11}, b_{22}, b_{33}, F_c)$$

Elastic Model for the saturated rock with solid and fluid pore infill:
Ciz and Shapiro (2007) theory

Fundamental Compressibilities

For **isotropic porous saturated media**, **Brown and Korringa (1975)** describe the changes in bulk V y and pore volumes V_p as a function of confining P_c and differential pressure P_d:

$$V(P_c, P_d), \quad V_p(P_c, P_d), \quad \text{where} \quad P_d = P_c - P_p$$

- **Drained bulk compressibility**

$$C_m = \frac{1}{K_m} = \frac{1}{V}\left(\frac{\partial V}{\partial P_d}\right)_{P_p} \qquad \text{(matrix)}$$

- **Unjacketed bulk compressibility**

$$C_{gr} = \frac{1}{K_{gr}} = -\frac{1}{V}\left(\frac{\partial V}{\partial P_p}\right)_{P_d} \qquad \text{(grains)}$$

- **Unjacketed pore compressibility**

$$C_\phi = \frac{1}{K_\phi} = -\frac{1}{V_p}\left(\frac{\partial V_p}{\partial P_p}\right)_{P_d} \qquad \text{(pore space)}$$

- **Undrained (closed) compressibility**

$$C^* = \frac{1}{K^*} = -\frac{1}{V}\left(\frac{\partial V}{\partial P_c}\right)_{m_f} \qquad \text{(closed)}$$

Fundamental Compressibilities and Compliances

- **Fluid compressibility**

$$C_f = \frac{1}{K_f} = -\frac{1}{\bar{V}_f}\left(\frac{\partial V_f}{\partial P_p}\right)_{m_f} \equiv S_f$$

- **Solid pore infill compressibility**

$$C_{if} = \frac{1}{K_{if}} = -\frac{1}{\bar{V}_P}\left(\frac{\partial V_{if}}{\partial P_p}\right)_{m_{if}} \equiv S_{if}$$

For Anisotropic Porous media

The compressibilities are generalized through **compliance tensors** in the form

$$\begin{array}{lcll} C_m & \longrightarrow & S^m_{ijkl}, & \text{(matrix)} \\ C_{gr} & \longrightarrow & S^{gr}_{ijkl}, & \text{(grains)} \\ C_\phi & \longrightarrow & S^{\phi}_{ijkl}, & \text{(pore space)} \\ C^* & \longrightarrow & S^*_{ijkl}, & \text{(closed)} \end{array}$$

For micro-homogeneous matrix

$$\mathbf{S}^{\phi} = \mathbf{S}^{gr}$$

Anisotropic compliance models

Brown and Korringa (1975) theory

In their classic paper they generalized Gassmann's equation and found the following relation for **multimineralic** matrix:

$$S^*_{ijkl} = S^m_{ijkl} - \frac{(S^m_{ij} - S^{gr}_{ij})(S^m_{kl} - S^{gr}_{kl})}{(S_m - S_{gr}) + \phi(S_f - S_\phi)}$$

Ciz and Shapiro (2007) equation

Extended BK formula for a porous solid with anisotropic **solid infill** in the form:

$$\boxed{S^*_{ijkl} = S^m_{ijkl} - (S^m_{ijmn} - S^{gr}_{ijmn})[\phi_E(S^{if} - S^\phi) + S^m - S^{gr}]^{-1}_{mnpq}(S^m_{pqkl} - S^{gr}_{pqkl}).}$$

Then we obtain the stiffness in the form

$$C^* = (S^*)^{-1}$$

Case study

Calibration of the model using well log data and cuttings from Inoceramus shale, Austral basin, Argentina

Inoceramus Formation, Austral Basin, Argentina

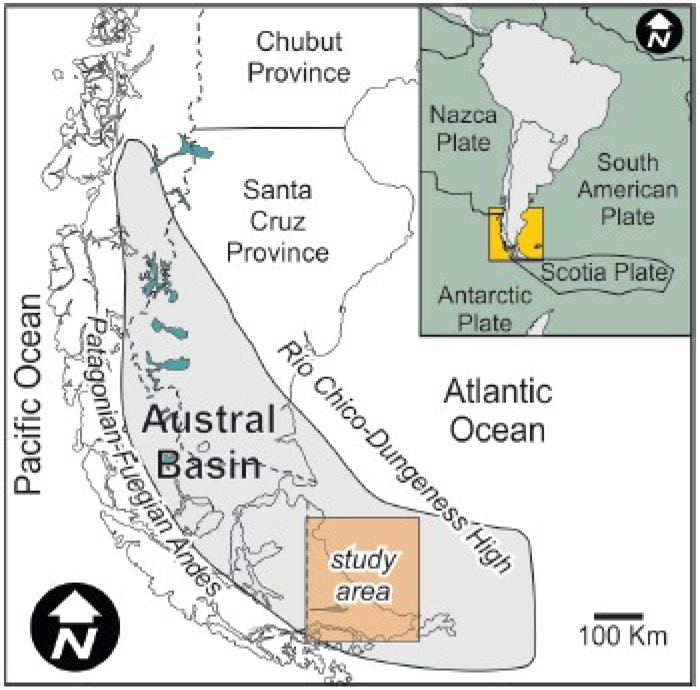

- Cretaceous *organic-rich* marine shales
- Net thickness from 150 to 200 m.
- Organic content TOC from 0.5 to 2.5%.
- Kerogen type II to III.
- Maturity: oil window.
- Data from two exploratory wells.
- Geologic formations: Margas Verdes and
  Pampa Rincón

Available Data

- **Well Logs**: dipolar sonic V_p, V_s, effective and total porosities, water saturation, density.

- **Pore pressure gradient** $\nabla P_p = 0.62\, psi/ft = 14\, MPa/km$

- **Measurements on cuttings**: X-ray diffraction (**DRX**): mineral fractions
  X-ray Fluorescence (**FRX**): Si, Al, Ca.
  Pyrolisis: total organic content **TOC**.

Also

- Estimation of Confining Pressure from density logs $\longrightarrow$ $P_c(z) = P_0 + \int \rho g\, z\, dz$

- Estimation of pore and differential stresses for each depth $\longrightarrow$ $P_p(z) = \nabla P_p\, z$

- Electrofacies: determined with TOC, FRX and velocities by means of clustering algorithm

3 main groups: Red (*carbonatic*), Blue (*Si/Al ratio*) and Green (*organic*)

Data from Well 1

Fm. **Inoceramus** inferior:

- Fm. Margas Verdes (MV)
- Fm. Pampa Rincón (PR)

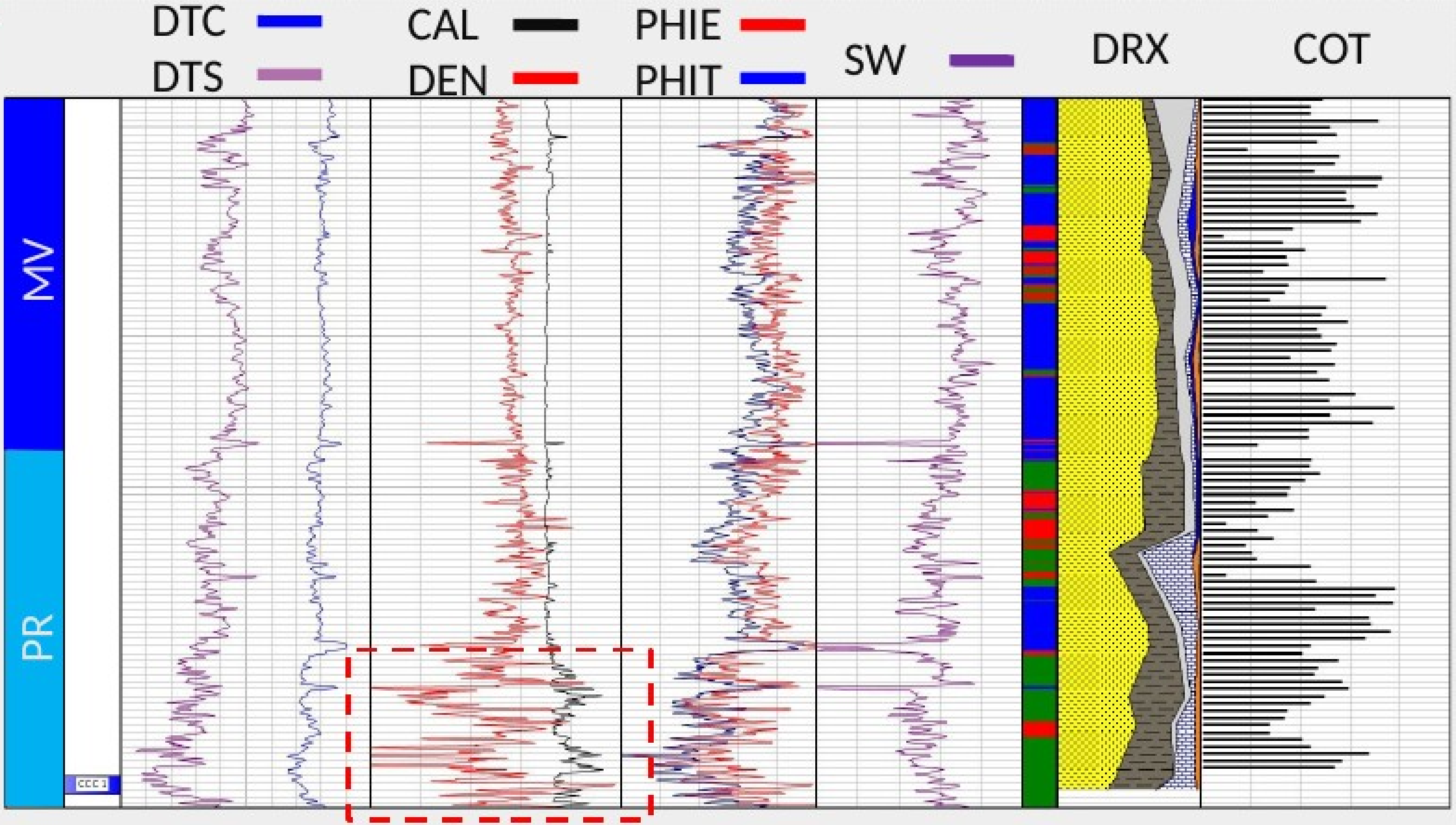

(8) Fracciones litológicas (DRX sobre recortes de perforación) (amarillo: Cuarzo, Gris oscuro con líneas negras: Arcillas, Gris claro: Plagioclasas, Ladrillos azules: Carbonatos, Azul sólido: Laumontita, Naranja: Pirita) (9) COT (Pirólisis sobre recortes de perforación).

Analogous data for Well 2

Fm. **Inoceramus** inferior:

- Fm. Margas Verdes (MV)
- Fm. Pampa Rincón (PR)

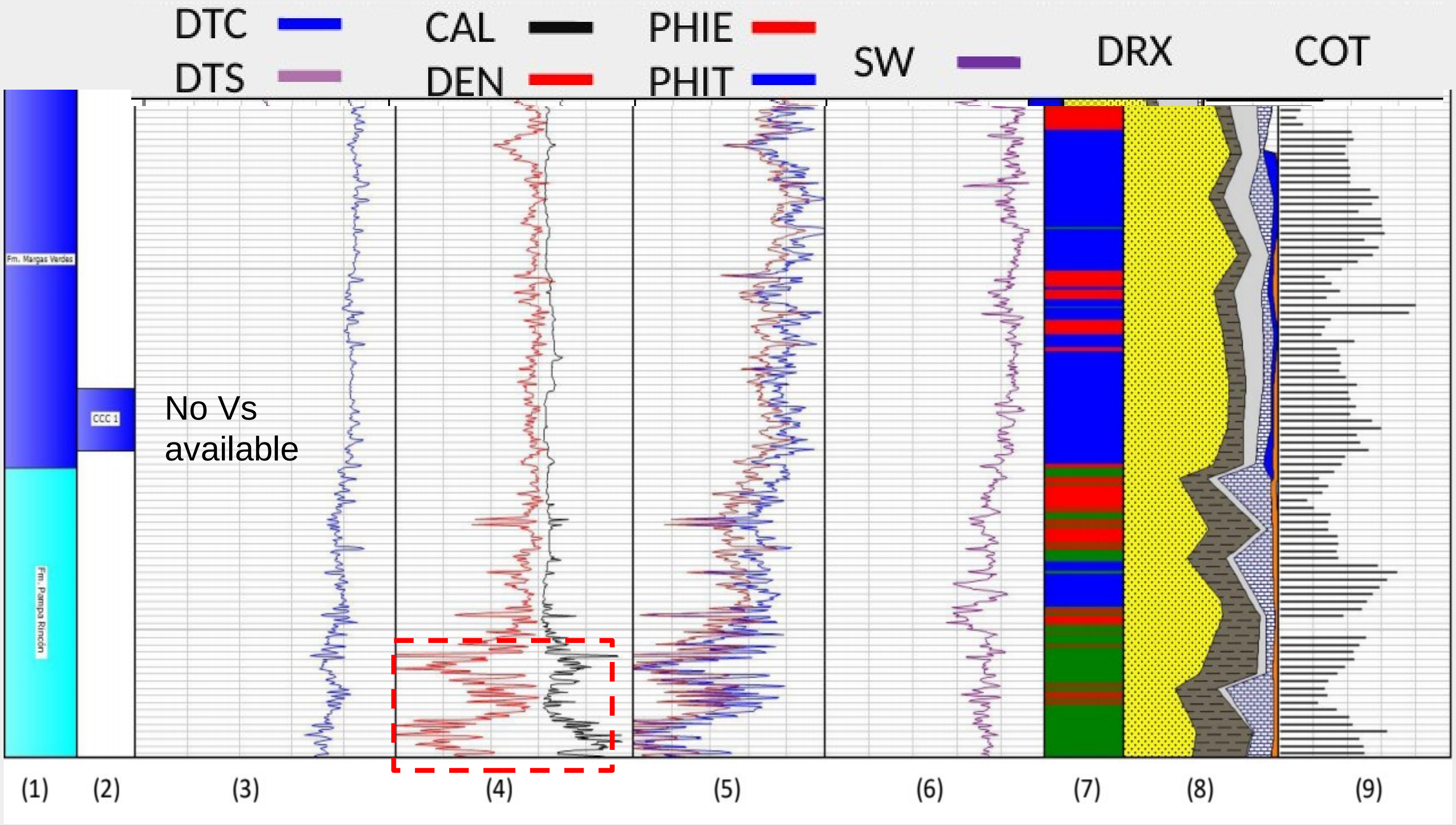

Conceptual model

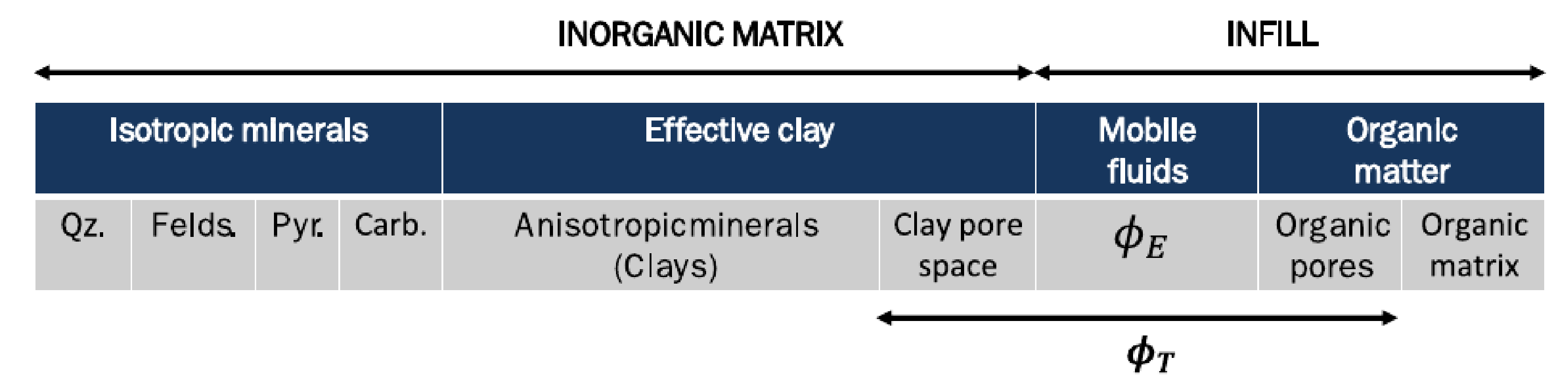

Step 1: Bulk density modeling and parameter inversion

Bulk density $$\hat{\rho} = (1-\phi_T)(1-K)\sum_{i=1}^{M}\rho_i f_i + \nu_k \rho_k + \phi_T \sum_{f=1}^{3} S_f \rho_f,$$

- the M **mineral phases** with volume fractions f_i: Quartz, Feldspar plg., Pyrite, Laumontite, Calcite and clays (Illite, Illite-Smectite, Smectite)
- the **kerogen fractions**

$$K = \frac{V_k}{V_m} = \frac{TOC\ \rho_{gr}}{C_k\ \rho_k} \quad \text{and} \quad \nu_k = \frac{V_k}{V} = \frac{K(1-\phi_E)}{1+K},$$

- the total porosity ϕ_T and effective porosity ϕ_E.
- the **pore fluids**: brine, oil, gas.
- the kerogen density ρ_k, the effective clay density ρ_{ec} and the constant C_k are inverted from measured bulk density.
- To do this, we find the minimum of the cost function given by

$$R(\mathbf{r}) = \left\| \hat{\rho}(\mathbf{r}) - \rho \right\|_2^2, \quad \text{where} \quad \mathbf{r} = (\rho_k, \rho_{ec}, C_k) \longrightarrow \textit{LMFIT Python package}$$

Step 2: effective elastic properties of the composite grains

INORGANIC MATRIX						INFILL		
Isotropic minerals				Effective clay		Mobile fluids	Organic matter	
Qz.	Felds.	Pyr.	Carb.	Anisotropic minerals (Clays)	Clay pore space	ϕ_E	Organic pores	Organic matrix

ϕ_T

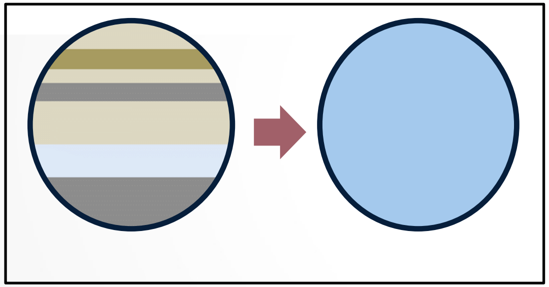

VTI matrix

Effective elastic properties of grains:

- Voigt-Reuss-Hill average of isotropic (non-clay) components
- Backus averaging: isotropic+anisotropic components $\longrightarrow S^{gr}$

From previous work

Pure Appl. Geophys. 179 (2022), 2437–2460

https://doi.org/10.1007/s00024-022-03049-1

Pure and Applied Geophysics

Check for updates

Stress-Dependent Anisotropic Rock Physics Modelling in Organic Shales of the Inoceramus Formation, Austral Basin, Argentina

Guido Panizza,[1,2] Claudia L. Ravazzoli,[1,3] and Emilio Camilión[2]

Abstract—We present an original anisotropic stress-dependent rock physics model for the organic rich shales of the Inoceramus formation, the main source rock and unconventional reservoir in

1. Introduction

We take clay elastic anisotropic properties from this study, based on ultrasonic measurements

Table 3

Optimized elastic properties and densities of the effective clay and of the kerogen in GPa and in kg/m^3

Optimized parameters	Effective clay									Kerogen			
	C_{33} [GPa]	C_{44}	C_{11}	C_{66}	C_{13}	ρ_c kg/m^3	ϵ	γ	δ	K_k [GPa]	μ_k	ρ_k kg/m^3	C_k
Well 1	37.5	10.6	62.4	14.4	13.2	2800	0.33	0.18	−0.08	4.85	4.36	1500	0.73
Well 2	35.3	6.9	66.	24.4	36.2	2300	0.43	1.26	0.52	3.	4.4	1460	0.77

C_k is the organic carbon concentration in the solid organic matter [Eq. (4)] and is dimensionless. ϵ, γ and δ are the Thomsen parameters for the optimized effective clay of each well and are dimensionless

Step 3: effective elastic properties of the pore infill

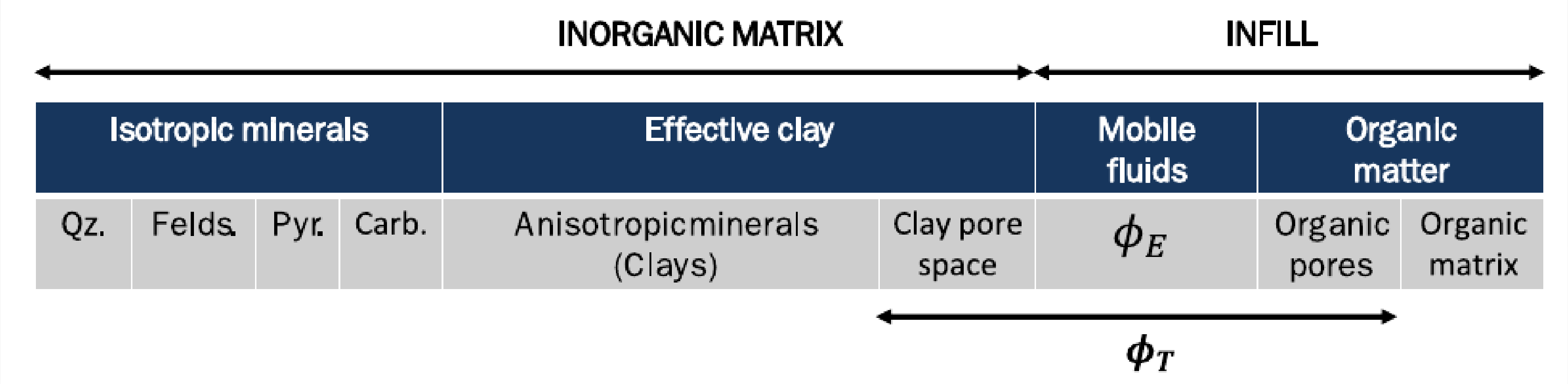

$$\phi_I = \phi_E + \upsilon_K$$

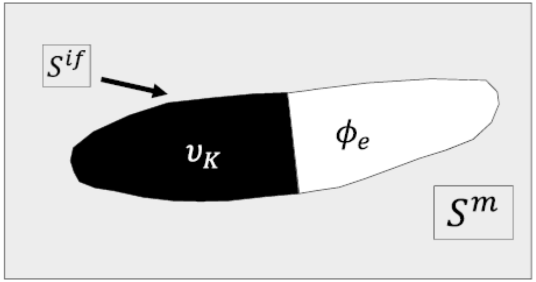

Effective elastic properties of the pore infill: Hashin-Shtrikman average kerogen + fluids → S^{if}

Step 4: Compressional and shear wave velocities and inversion of PDA matrix parameters

Computation of synthetic anisotropic velocities using S^* and $\hat{\rho}$

To compute vertical velocities we take $\theta = 0$ we use the stiffness C^*_{ij} and the bulk density in

$$\hat{v}_p(\theta) = (C^*_{11} sin^2(\theta) + C^*_{33} cos^2(\theta) + C^*_{44} + \sqrt{M})^{1/2}(2\hat{\rho})^{-1/2}$$
$$\hat{v_{sv}}(\theta) = (C^*_{11} sin^2(\theta) + C^*_{33} cos^2(\theta) + C^*_{44} - \sqrt{M})^{1/2}(2\hat{\rho})^{-1/2}$$
$$M = \left[(C^*_{11} - C^*_{44}) sin^2(\theta) - (C^*_{33} - C^*_{44}) cos^2(\theta)\right]^2 + (C^*_{13} + C^*_{44})^2 sin^2(2\theta)$$

Inversion of the matrix PDA parameters

To determine the PDA fitting parameters

$$\mathbf{m} = (a_{11}, a_{13}, a_{33}, a_{44}, a_{66}, b_{11}, b_{22}, b_{33}, F)$$

we minimize the differences between measured and model velocities in the form

$$Q(\mathbf{m}) = \sum_{k=1}^{N} \left\| L^{(k)}(\mathbf{m}) \right\|_2^2, \quad \text{where} \quad L^{(k)}(\mathbf{m}) = \begin{pmatrix} \hat{v}_p^{(k)}(0^\circ, \mathbf{m}) - v_p^{(k)}(0^\circ) \\ \hat{v}_s^{(k)}(0^\circ, \mathbf{m}) - v_s^{(k)}(0^\circ) \end{pmatrix}$$

Acceptance conditions: energy inequalities.

Results: PDA parameters

We solve different inverse problems using the data set corresponding to each electrofacie, however only the exponent F_c parameter showed differences.

Formación	a_{11}	a_{33}	a_{44}	a_{66}	a_{13}	b_{11}	b_{22}	b_{33}
	$\times 10^{-2}$ [GPa^{-1}]					$\times 10^{-4}$		
Margas Verdes	2.124	2	10	6	-0.41	2.9	0.054	5.96
Pampa Rincón	2.556	2.722	10.88	6.67	-0.822	0.186	0.	9.557

Table 1: Optimum values of PDA matrix model for each formation and both wells.

F_C	Electrofacie		
	1: Red	2: Blue	3: Green
Pozo 1	0.389	0.327	0.319
Pozo 2	0.659	0.621	0.304

Table 2: Optimized values of F_C for each electrofacie in MPa^{-1}.

Results: density and velocity logs Well 1

Well 1

$$E_\rho = 2.25\%$$

$$E_{v_p} = 4.1\%$$

$$E_{v_s} = 6.4\%$$

Mean Relative Cuadratic Error

$$E(\mathbf{m}) = 100 \times \sqrt{\frac{1}{N}\sum_{k=1}^{N}\left(\frac{\hat{x}^{(i)}(\mathbf{m}) - x^{(i)}}{x^{(i)}}\right)^2}.$$

Bulk density

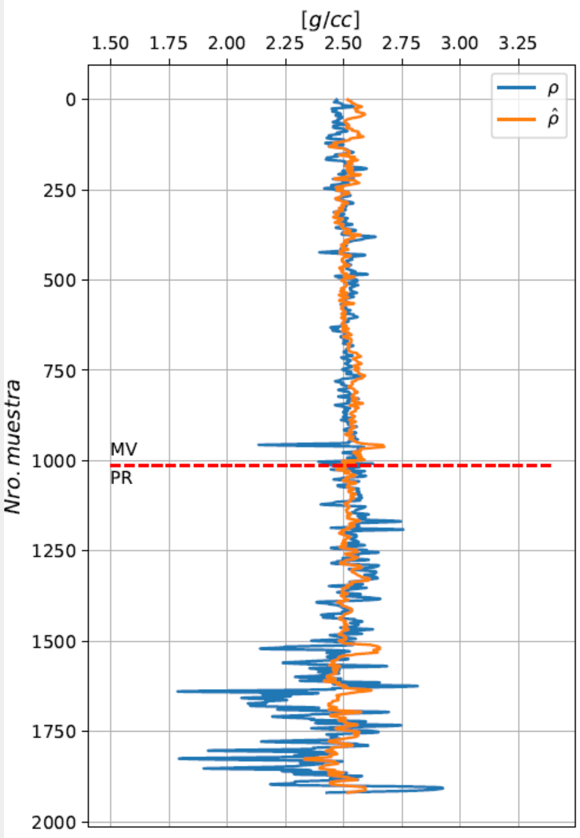

Vertical Vp and Vs

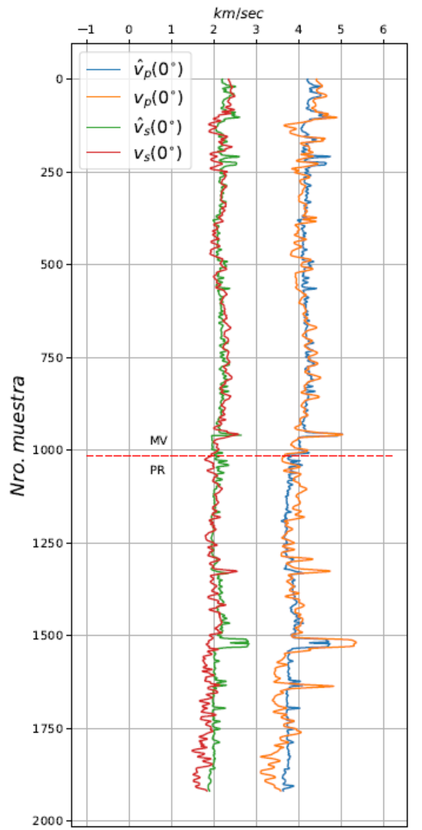

Results: density and velocity logs Well 2

No shear velocity log at well 2

$$E_\rho = 1.2\%$$

$$E_{v_p} = 4.7\%$$

Bulk density

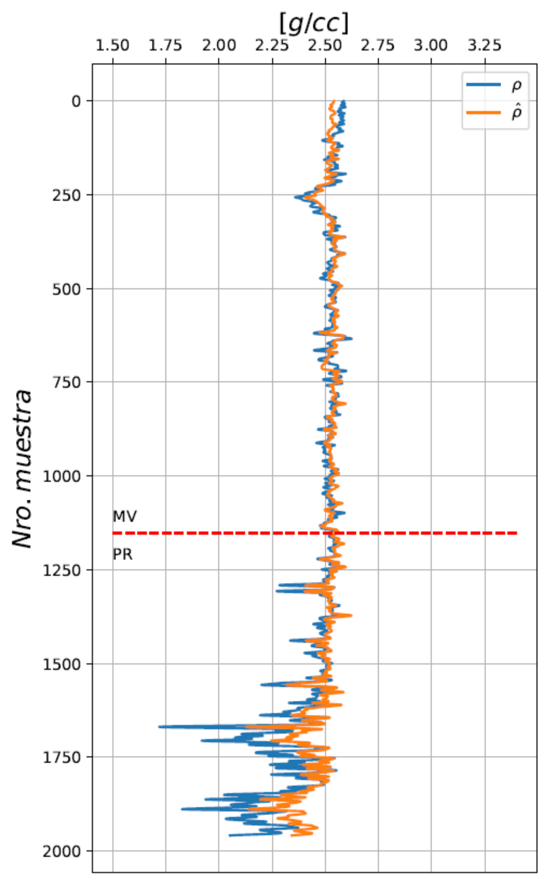

Vertical Vp, Vs

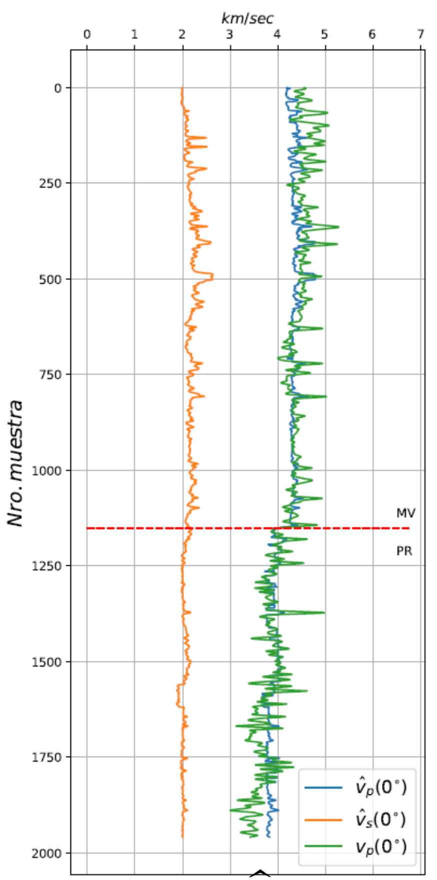

estimated $\hat{v}_s$

Thomsen's anisotropy parameters

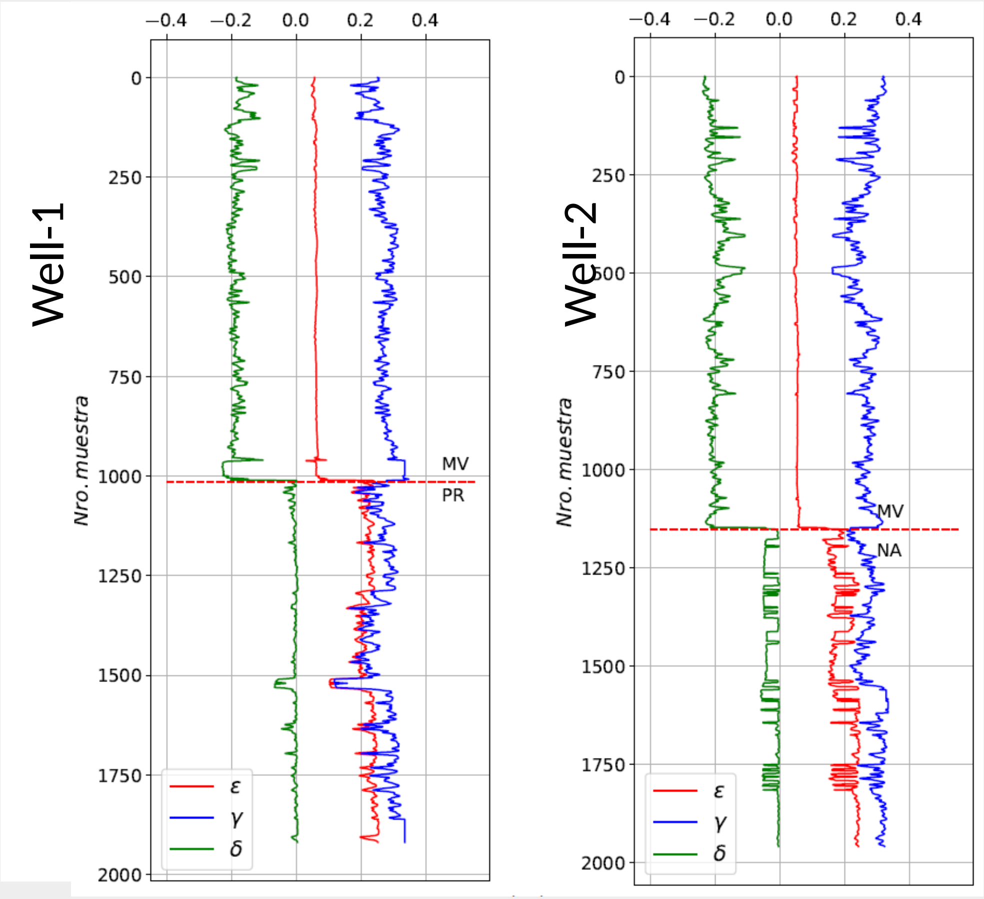

ε

δ

γ

$$\epsilon = \frac{C_{11} - C_{33}}{2C_{33}}$$

$$\gamma = \frac{C_{66} - C_{44}}{2C_{44}}$$

$$\delta = \frac{(C_{13} + C_{44})^2 - (C_{33} - C_{44})^2}{2C_{33}(C_{33} - C_{44})}$$

$\delta \approx 0$

In Pampa Rincón Fm.
ANNIE three parameter model would be fine, (Schoenberg et al. 1996)

Isotropic and anisotropic (dynamic) Young modulus

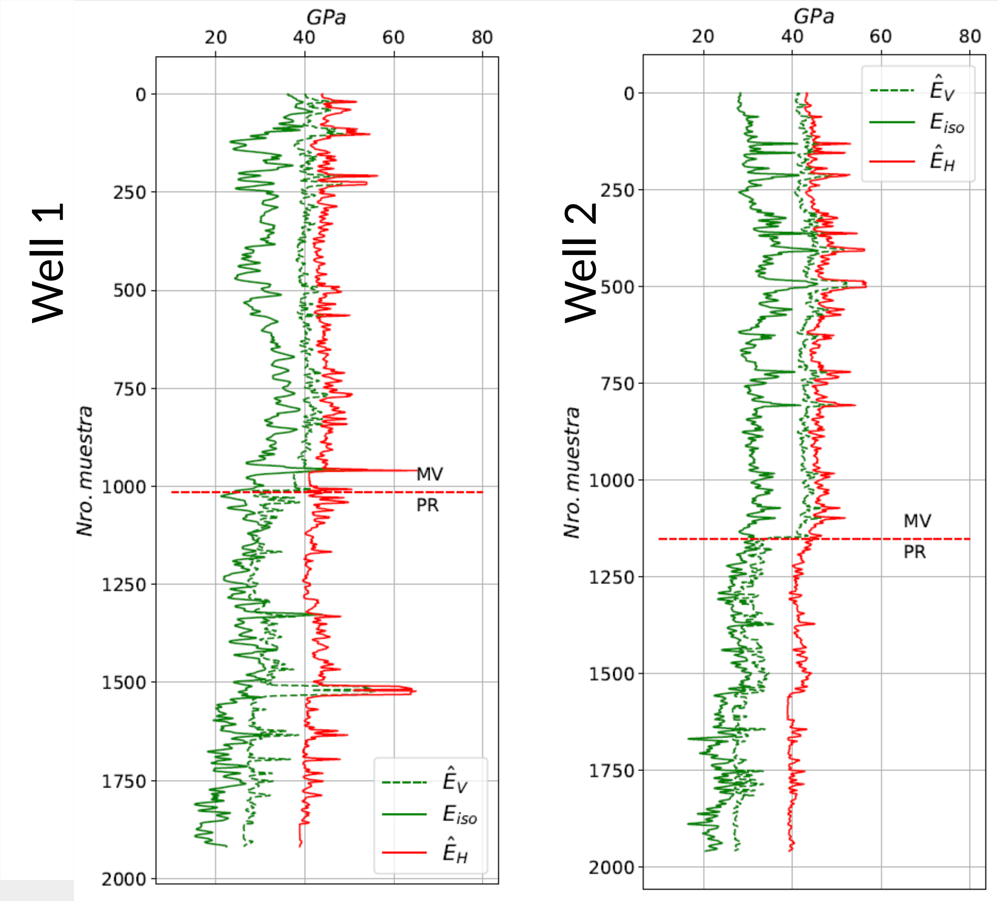

30 % de diferencia entre

E_V y E_{iso} en MV

20 % de diferencia entre

E_V y E_{iso} en PR

Sensitivity of Poisson ratio to TOC

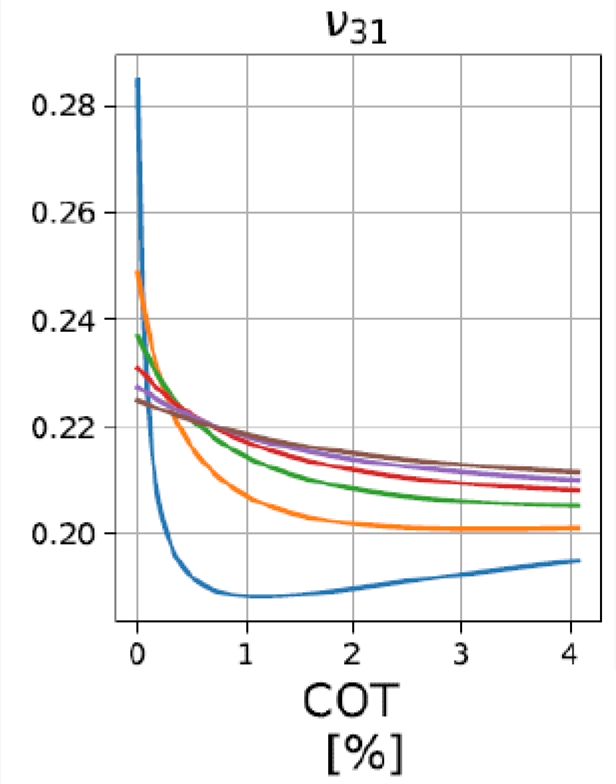

Módulos de Poisson

$$\nu_{ij} = -\frac{\epsilon_{jj}}{\epsilon_{ii}}$$

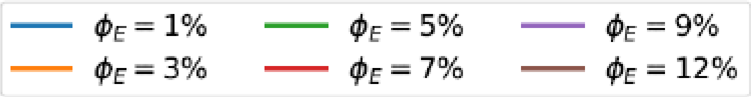

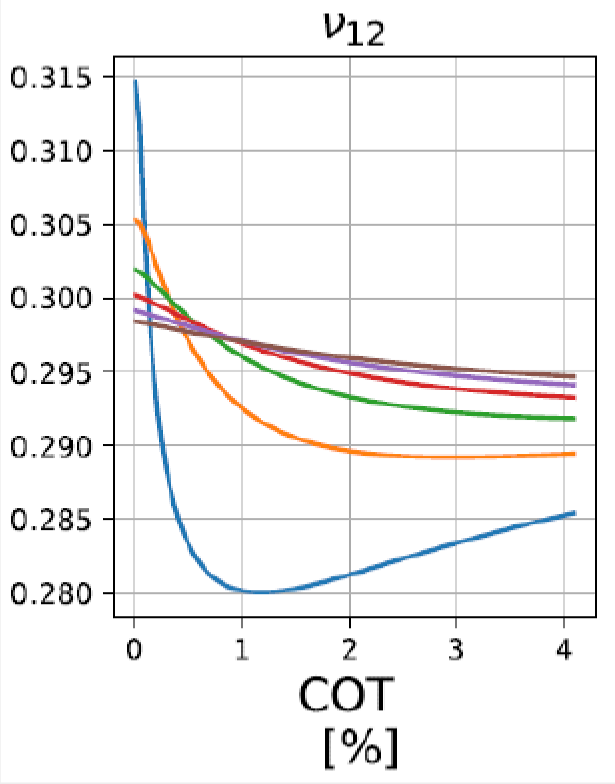

Sensitivity of Young modulus to TOC

Módulos de Young

$$E_{ii} = \frac{\sigma_{ii}}{\epsilon_{ii}}$$

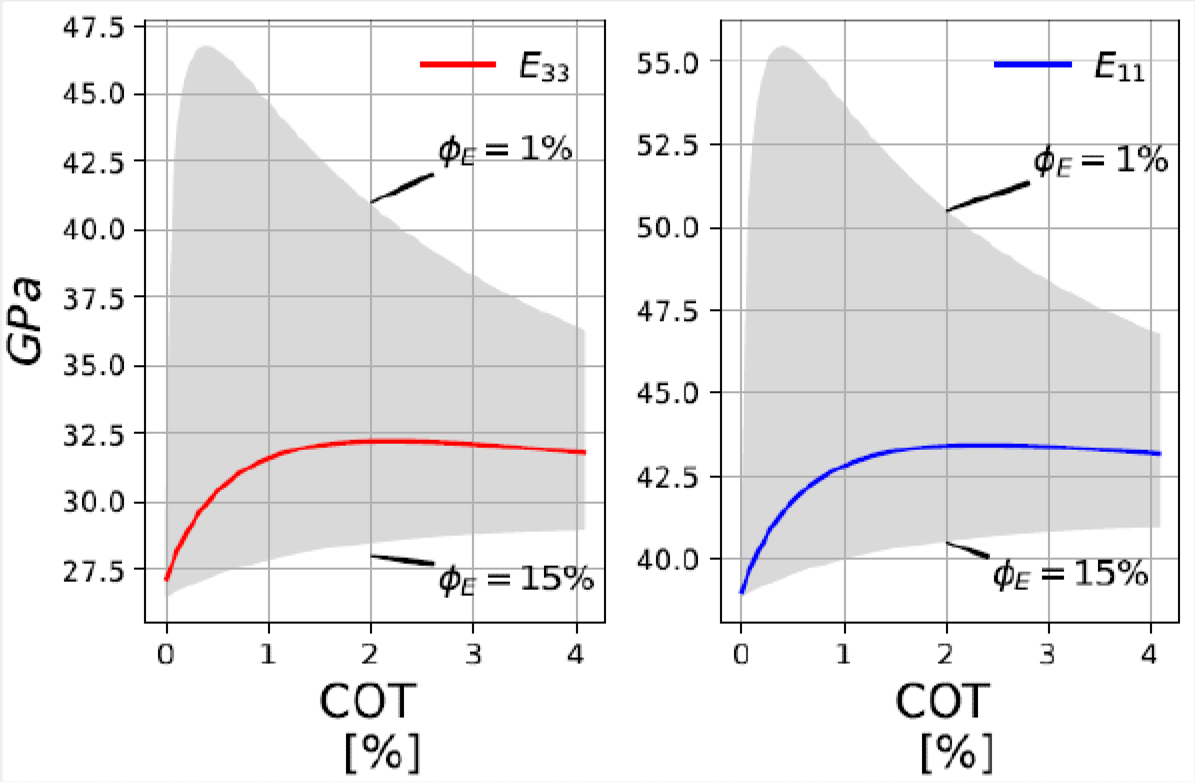

To conclude

The calibrated models can be useful for applications such as:

- Control of well velocities to detect and replace "erroneous" or missing data in damaged intervals,
- Anisotropy parameters,
- Estimation of shear velocities,
- Estimation of geomechanic coefficients,
- Reflection coefficients,
- Fluid and solid substitution,
- Simulation of synthetic seismograms and other attributes,
- Sensitivity analysis.

Thanks for your attention,
and

Muchas Felicidades Juan